2016

Analysis of Indicator Diagrams of a Water Injected Twin-shaft Screw-type Expander

Alexander Nikolov
Chair of Fluidics, TU Dortmund University, alexander.nikolov@tu-dortmund.de

Andreas Brümmer
Chair of Fluidics, TU Dortmund University, andreas.bruemmer@tu-dortmund.de

Analysis of Indicator Diagrams of a Water Injected Twin-shaft Screw-type Expander

Alexander NIKOLOV*, Andreas BRÜMMER

Chair of Fluidics, TU Dortmund University,
Dortmund, Germany
alexander.nikolov@tu-dortmund.de
andreas.bruemmer@tu-dortmund.de

* Corresponding Author

ABSTRACT

Twin-shaft screw-type expanders offer a high potential for energy conversion in the lower and medium power range, for instance as expansion engines in Rankine cycles for exhaust heat recovery. With regard to minimizing internal leakages and lubricating moving machine parts, an auxiliary liquid or liquid working fluid, for example in organic Rankine cycles (ORC)[1], can be fed to the screw expander.
In this paper, indicator diagrams of a twin-shaft screw-type expander prototype SE 51.2 designed at the Chair of Fluidics at TU Dortmund University are presented and analyzed in detail. The experimental investigations are carried out on a hot-air test rig with an expander inlet manifold water injection. The time-dependent working chamber pressure is recorded by means of high-resolution absolute pressure transmitters. Hereby, specific aspects of working chamber pressure measurements are mentioned. Based on the indicator diagrams, relevant influence mechanisms on the expander's operational behavior resulting from water injection are determined. Additionally, the impact of the injected water on the expander's delivery rate and mechanical efficiency is presented.

1. INTRODUCTION

Due to the growing shortage of non-renewable fossil fuel reserves and the resulting increase in primary energy costs, little developed energy potentials increasingly move into the focus of economic interest. Available heat sources in the field of decentralized energy systems of small and medium power ranges, such as industrial exhaust gases or waste heat in vehicles' engines, geothermal or solar thermal energy can be converted into useable mechanical power by means of expanders or turbines within a Rankine cycle.
In this context, twin-shaft screw-type expanders in Rankine cycles possess clear advantages compared with turbo machines or even other expander concepts. In general, twin-shaft screw-type machines are characterized by relatively high energy density and efficiency, good part load behavior, and rather a simple design. Furthermore, screw expanders in Rankine cycles are suitable for wet-vapor operation, so that an overheating system is not essential. On the one hand, the number of ORC components and the overall system costs can be reduced. On the other hand, liquid in screw expanders is even beneficial with regard to minimizing internal leakages and reducing noises or vibrations.
Whereas injecting oil is a common method in screw-type compressors without timing gears, water as an auxiliary fluid offers sufficient potential for investigation. There are commercial water injection concepts for screw-type compressors with timing gears which aim to reduce gas temperature and thermal stress in the working camber. Investigations of water and oil injection into screw-type expanders with timing gears were done by Zellermann (1996). Rinder *et al.* (2004) presented benefits and disadvantages of water compared to oil injection with regard to a screw-type compressor without timing gears. Furthermore, Rinder and Moser (1990) have shown oil distribution in a screw compressor. Kliem (2005) investigated a screw expander application in a trilateral flash

[1] (Organic) Rankine cycles are thermodynamic cycles that operate as a closed loop. In Rankine cycles an operating fluid, water or organic fluid, is continuously pressurized, evaporated, expanded and eventually condensed.

cycle theoretically and experimentally. Here, overheated water is injected into the working chamber where it expands and evaporates. An approach for the theoretical investigation of screw expanders in trilateral flash cycles is presented by Vasuthevan and Brümmer (2016). An application of screw-type expanders in trilateral flash cycles is predicted to be a promising approach in the medium and low power operating range in ORC by Ohman and Lundqvist (2015).

In order to determine hydraulic friction losses in screw expander clearances using an auxiliary liquid, an analytical approach was presented by Gräßer and Brümmer (2014) with regard to water and by Gräßer and Brümmer (2015) to oil. Nikolov and Brümmer (2014) presented a water injected screw-type expander, focusing on an integral investigation of the test expander without differentiation between the impact mechanisms resulting from the auxiliary fluid. The most important expected advantage of water injection into screw-type expanders is sealing of clearances as well as lubrication of the hardened and hard-coated screw rotors during operation. At the same time depending on the liquid injection temperature, the auxiliary fluid lifts the temperature level within the working chamber due to its higher heat capacity. Compared to a dry-running expander, injected water reduces temperature drops during expansion which result in a slight difference between the inlet and outlet temperature of the working fluid, as well as lower thermal stress alongside the expander.

Kovacevic and Rane (2013) presented a 3D analysis of a twin screw expander. Indicator diagrams, mass flow rates and expander power at different operating conditions were estimated and compared with experimental results.

Cao *et al.* (2011) presented the results of an experimental investigation of pressure distribution inside the working chamber of a twin screw compressor for multiphase duties. Additionally, a mathematical model for describing the pressure distribution inside the working chamber is proposed.

Within the framework of the following paper, indicator diagrams of a water injected screw expander are presented. Based on the indicator diagrams, relevant influence mechanisms on the expander's operational behavior resulting from water injection are determined and explained in detail.

2. EXPERIMENTAL SETUP

The experimental rig, measurement devices which were used, and the test screw-type expander are introduced below. In addition, an overview of the test parameters is given.

Diverse measurement devices record information about the fluid state in the rig and the test screw-type expander. Insulated thermocouples and static relative pressure transducers are installed at different points of the test rig. Mean static pressure and temperature of the gaseous working fluid is metered in the test rig before water injection. Inlet and outlet static pressure as well as overall fluid temperature is recorded both in the high and low pressure domains of the test expander. The effective power of the test screw-type expander is calculated by means of rotational speed and driving torque metered using a torque transducer.

Within the framework of this paper, the results of experimental investigations on a water injected screw-type expander SE 51.2 without timing gears (Figure 1) are presented. The expander’s geometrical parameters are listed in Table 1. SE 51.2 is a further development of a twin screw charger GL 51 designed at Chair of Fluidics by Temming (2007). The screw rotors are hardened and have a tough wear-protection coating, so that seizure can be avoided at dry running or water injection. Both fixed and loose bearing sets are grease lubricated, so that no oil supply is necessary. To avoid water flow through the fixed bearing sets on the high pressure expander side and protect them from damage, a pressure cushion at constant level near the expander’s inlet conditions is set by a pressurized air in the coupling casing.

In the high pressure domain of SE 51.2, a variable plate, which is shaped like the inlet control edge, is used. Thus, the inner volume ratio and the utilizable pressure ratio can be adjusted. Moreover within the framework of experimental investigations, inlet throttling effects can be investigated in detail. However, the inner volume ratio is set constant for the experimental results presented below. Due to its modular structure, the geometry parameters of the screw-type expander SE 51.2 can easily be modified. Apart from front clearance heights, housing and intermesh clearance heights can be varied by changing the corresponding expander module.

In order to have a more detailed look into the physical effects of liquid phase within the working chamber, indicator diagrams for dry- and wet-running operation of SE 51.2 are recorded by means of six high-resolution absolute piezo-resistive pressure transmitters, Figure 1. Hereby, two different sensor types and sizes are used, which are installed flush with the rotor bore surface and at the high-pressure front side. The pressure transmitters of the series M5 manufactured by “KELLER AG für Druckmesstechnik” at positon 0, 1 and 6 record the static pressure at the inlet port (position 0), within a rotational angle in the range between 85° and 130° (position 1) and during the fluid discharge on the low pressure side of the expander (position 6). Each of these three sensors delivers the absolute pressure at the metering point. With regard to the manufacturer’s data sheet of these transducers, a resonance

frequency of more than 50 kHz can be expected. Nevertheless, a small cavity at sensor tip is constructively available. Therefore especially at water injection, acoustical Helmholtz resonances may occur as a result of the rotor tip gliding at the sensor. In this case, dynamic effects induce an impulse which can excite strong resonance oscillations at frequencies far lower than given natural frequency in the sensor data sheet. This aspect has to be considered within the evaluation of the pressure signal in order to avoid inaccurate interpretation. However, this sensor type is essential for the experiments to record the working chamber pressure for very small chamber volume at sensor position 1 in the high pressure front section, where an extremely narrow mounting space in the expander's casing is available.

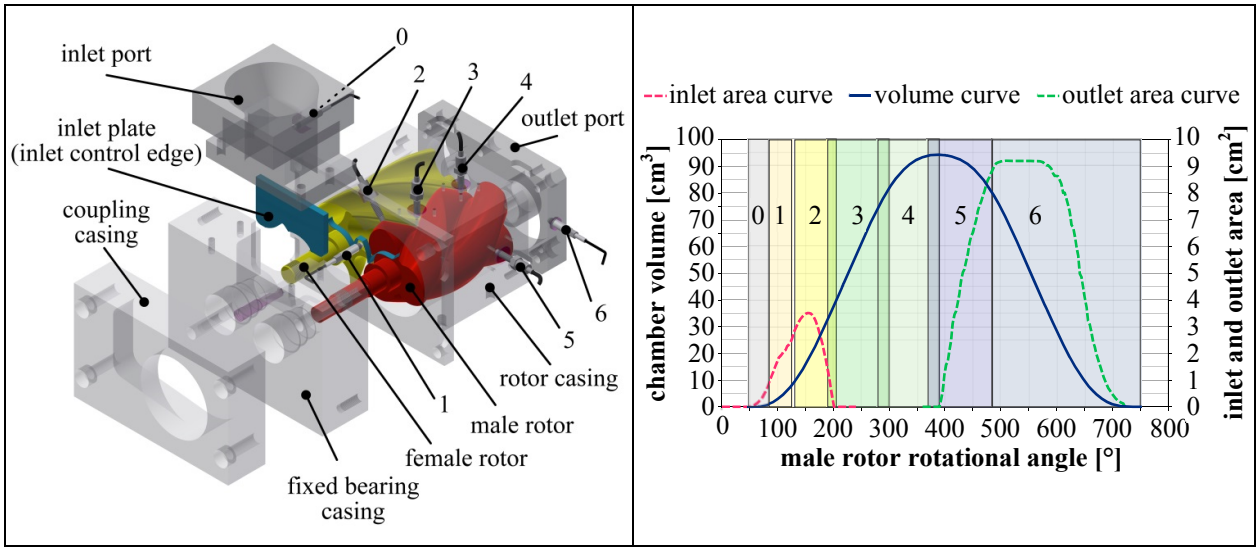

Figure 1: Positions of pressure indication transmitters (0…6), inlet and outlet area, as well as volume curve of the test screw expander SE 51.2

At positon 2 to position 5 XTM-190 pressure transducers manufactured by "Kulite Semiconductor Products, Inc" with natural frequency higher than 425 kHz are mounted flush with the rotor bore surface and have no dead space between their tip and the considered working chamber. Hence, no acoustic issues at the metering point with regard to acoustic Eigen frequencies are expected. Within the calibration of these sensors, the pressure sensitivity proved to be nearly constant. However, a relatively great temperature depending offset could be observed. Hence, insulated thermocouples are installed at each pressure measurement position in order to compensate the impact of temperature changes on the sensor sensitivity.

Table 1: Parameters of the test screw expander SE 51.2

designation	**unit**		**designation**	**unit**	**male rotor**	**female rotor**
axis-center distance a	[mm]	51.2	number of lobes z	[-]	3	5
internal volume ratio v_i	[-]	2.5	diameter d	[mm]	71.8	67.5
displaced volume per male rotor rotation V	[cm^3]	286	wrap angle φ	[°]	200	-120
front clearance height $h_{fc,hp}$ (high pressure)	[mm]	0.1	rotor lead s	[mm]	181.8	-303
front clearance height $h_{fc,lp}$ (low pressure)	[mm]	0.17	rotor length l	[mm]	101	
housing clearance height h_{hc}	[mm]	0.08	rotor profile	[-]	modified asymmetric SRM	

Due to relatively high temperature sensitivity and offset of this sensor type, only the relative change in pressure to a reference pressure level is considered. At this point, the reference pressure is determined at the overlapping scope of two adjacent transducers (Figure 1). To begin with, the static pressure in the outlet port of the screw expander is considered as the starting reference pressure.

Within the scope of this indication pressure measurement, a rotational angle range between 130° and 140° cannot be covered due to lack of space in the casing, so the pressure has to be estimated. Preliminary analysis of the recorded pressure delivered a linear pressure distribution in the missing range to be qualitatively and quantitatively sufficiently accurate. For the area which was not surveyed at the beginning of the working cycle from 45° (start of

chamber filling) to 85° as shown in Figure 1, the dynamically recorded inlet port pressure is considered identical to the chamber pressure. In this way, the assumed chamber pressure is mapped with regard to an ideal chamber filling without pressure drop over the inlet. In theory, this results in an upper limit for the converted internal working of the screw expander within this working cycle range. Another approach to map the chamber pressure profile in this section is to assume a linear pressure increase starting from the outlet and ending at the pressure level of the transmitter at position 1. This method is more appropriate with respect to increasing inlet throttling losses either at higher expander's rotational speed or increasing amount of injected water. Therefore, the pressure level and the induced inner work within the missing range of the indicator diagram are expected to be lower than the real one during the chamber growth. This approach represents a lower limit for the converted inner work within the first 40° of chamber formation between 45° and 85°.

The relation between the time dependent high-resolution pressure signals and rotational angle and chamber volume is provided by an optical trigger mounted on the male rotor shaft. Thereby, a TTL impulse is generated once per male rotor revolution, which corresponds to a defined position of both rotors in relation to each other and the working chamber volume. Between two trigger signals, an equidistant correlation between time and rotational angle axis is considered. In terms of sufficient high resolution of the time depending signals, a sampling rate of 100 kHz with regard to pressure transducers and trigger signal is provided.

Within the framework of this experimental investigation, both the system and the screw expander's operating parameters were varied. Water was injected at temperature levels of $\vartheta_{i,w} \approx 30$ °C, $\vartheta_{i,w} \approx 60$ °C, and $\vartheta_{i,w} \approx 90$ °C for a constant air inlet pressure of $p_i = 4 \cdot 10^5$ Pa and back pressure of $p_o = 1 \cdot 10^5$ Pa and at hot air temperature of $\vartheta_{i,a} = 90$ °C. The resulting mixture temperature at the expander's inlet is $\vartheta_i < 40$ °C, $\vartheta_i \approx 50$ °C, and $\vartheta_i > 60$ °C respectively depending on water volume flow and expander rotational speed.

With regard to steam or vapour mass fraction, the amount of injected water into the expander's inlet port is represented by the relative air mass fraction related to the overall air and water mass flow:

$$x = \frac{\dot{m}_a}{\dot{m}_a + \dot{m}_w}. \tag{1}$$

Here, measured air mass flow $\dot{m}_a$ (Coriolis mass flow meter) corresponds to almost dry air, since a refrigerant type dryer is used after air compression. Air mass fraction of $x = 1$ corresponds to a dry-running operation and $0 < x < 1$ to water injection operation and a two-phase flow respectively. The air mass fraction x is varied in the range from 1.0 to 0.4 depending on water temperature and expander's rotational speed. For water injection, two nozzle sizes are used at two adjacent water flow ranges with respect to a satisfactory water injection quality at the expander's inlet. The maximum expander rotational speed is $n_{MR} = 18{,}000$ min^{-1}, which equals a male rotor circumferential speed of $u_{MR} = 67.7$ m·s^{-1}.

3. CHARACTERISTIC NUMBERS

The operational behaviour of screw-type expanders is evaluated by means of characteristic numbers. Effects such as the sealing of expander clearances, inlet pressure drops, hydraulic losses, etc., can be evaluated integrally by taking the system and expander operating parameters into account. The characteristic numbers used here are delivery rate and mechanical efficiency.

3.1 Delivery Rate

Delivery rate is a characteristic number which describes different loss mechanisms such as internal or external leakages, inlet pressure drops during the chamber filling, or thermal effects within a displacement machine. For a screw-type expander, delivery rate is defined as:

$$\lambda_L = \frac{\dot{m}_a}{\dot{m}_{th}}. \tag{2}$$

Here, $\dot{m}_{th}$ represents theoretical air mass flow with:

$$\dot{m}_{th} = V_{th,ex} \cdot \rho_{da,i} \cdot n_{MR} \cdot z_{MR}. \tag{3}$$

The parameters z_{MR} and n_{MR} correspond to male rotor lobes and male rotor rotational speed respectively. Displaced chamber volume by the liquid can be ignored due to a relatively high volume fraction of air, at over 98.5 % even at the lowest air mass flow and highest injected water volume flow rate. The parameter $V_{th,ex}$ refers to chamber volume after completing the chamber filling. Moreover, dry air is regarded as an ideal gas and its density $\rho_{da,i}$ is considered with reference to calculated subcooled temperature after water was injected. In terms of delivery rate, measured air mass flow $\dot{m}_a$ does not consider evaporated water steam with respect to saturated humid air after water injection, because the Coriolis mass flow meter is installed upstream of the water injection nozzle. In some cases at high temperature levels and low pressure at the same time, evaporated steam fraction has to be taken into account, since it significantly increases. Within the following investigations, steam mass flow increases up to 4.7 % of metered air mass flow at the highest injected water temperatures. Since steam mass flow is not measured by the Coriolis flow meter, an additional decrease of delivery rate of a maximum of 4.7 % is determined at some operating points.

3.2 Mechanical Efficiency

Mechanical efficiency η_m is a characteristic number, which gives information about the amount of mechanical and hydraulic friction losses in screw expanders relating effective and indicated power to each other:

$$\eta_m = \frac{P_e}{P_{ind}}. \tag{4}$$

Effective power results from the recorded expander's rotational speed and torque:

$$P_e = 2 \cdot \pi \cdot n_{MR} \cdot M_{MR}. \tag{5}$$

Indicated power can be calculated by means of time-dependent working chamber pressure p and volume V, male rotor rotational speed n_{MR} and number of male rotor lobes z_{MR} as follows:

$$P_{ind} = - n_{MR} \cdot z_{MR} \cdot \oint p \cdot dV. \tag{6}$$

Within the investigated screw expander, friction losses P_ϕ result from the contact between both screw rotors, in the bearings, in sealing elements, as well as from hydraulic friction of the injected auxiliary fluid within clearances and at rotor surfaces. Friction losses can be calculated by means of Equation (7) as follows:

$$P_\phi = P_{ind} - P_e. \tag{7}$$

4. INDICATOR DIAGRAMS

In the following section, indicator diagrams of the test screw expander are presented for dry-running and water-injection operation. Indicator diagrams deliver an insight into the inner fluid-mechanical and frictional effects of the test screw expander. Statements about inner dissipative mechanisms during each working cycle are thus possible with reference to the chamber pressure distribution per working cycle. Hereby, relevant effects of water injection on the chamber state as well as specific issues concerning the interpretation and evaluation of locally recorded pressure levels are considered. Each indicator diagram, presented in the following, is calculated by averaging the chamber pressure of all resulting working cycles within a given time frame of one second at a rotational speed of 500 min^{-1} and 0.5 s at higher rotational speeds.

4.1 Dry-running Operation

In the following, the chamber pressure dependency on the expander's rotational speed for an inlet pressure of $4 \cdot 10^5$ Pa and temperature of 90 °C is examined, Figure 2. In addition to chamber pressure, the measured signals of the dynamic pressure transducer at position 0 in the inlet port are depicted.

The chamber pressure at male rotor circumferential speeds of $u_{MR} = 9.4$ m·s^{-1} (n = 2,500 min^{-1}), $u_{MR} = 22.6$ m·s^{-1} (n = 6,000 min^{-1}), and $u_{MR} = 67.7$ m·s^{-1} (n = 18,000 min^{-1}) is illustrated. Two significant mechanisms according to the operation of screw expanders can be observed. On the one hand, internal leakages at lower rotational speeds impact the chamber pressure in the range of male rotor rotational angle between nearly 200° and 390°. On the other

hand, inlet throttling losses increase at higher rotational speed, whereas the internal leakages decline due to the reduced working cycle period. Internal leakages decrease at operating points with higher rotational speeds because less time is available for the mass exchange between the working chambers.
Particularly remarkable is the decreasing chamber pressure level up to a rotational angle of 200° at high rotational speeds. According to Equation 8, flow velocity has a greater influence on the throttling losses than the inlet density, since the inlet pressure losses do not increase linearly but by the square of flow speed:

$$\Delta p_{\phi} = \zeta \cdot \rho \cdot \frac{c^2}{2}. \tag{8}$$

The relation between increasing inlet throttling and declining internal leakages at high rotor circumferential speed results in overexpansion, which means that the chamber pressure expands lower than the backpressure level.

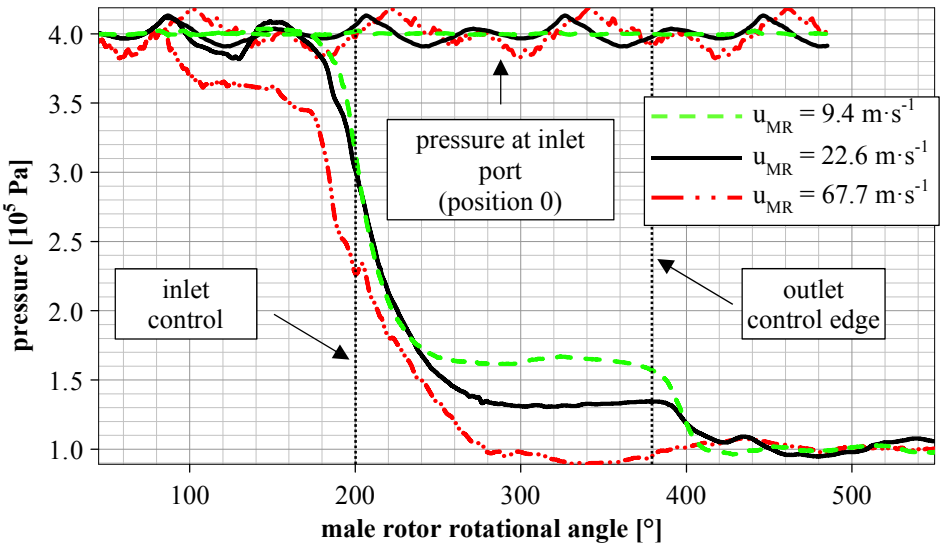

Figure 2: Indicated working chamber and inlet port pressure depending on male rotor rotational angle at an inlet pressure of $4 \cdot 10^5$ Pa and temperature of 90 °C and different male rotor circumferential speeds (no water injection)

Obviously, a periodic pressure pulsation specific for volumetric displacement machines can be detected at the high and low pressure port of the screw expander. The amplitude of the pulsations increases at higher rotational speeds. The recorded pressure pulsations in the inlet port at position 0 are comparable in amplitude and phase with those in the working chamber while it is connected to the inlet port. Thus, an impact of this pressure pulsation can be expected within the working chamber unless it is not disconnected from the inlet port. This effect is known in the literature as resonance charging. Depending on the phase of the oscillations, the chamber filling might be affected differently. Hereby, a local pressure distribution, possibly related to an acoustic standing wave, can be expected. The pressure recorded by the pressure transducers is presumably only a local instantaneous value. Here, a local pressure differing from the mean chamber pressure is possible. Last but not least, the transient inflow into the working chamber and cross-sectional jump over the inlet offer potential for vortices and separated flow regions in the chamber while it is connected to the inlet port. In this way, the mapping of the indicator diagram can lead to deviation from the real inner power, which has to be considered.

4.2 Water Injection

Variation of injected water is carried out in terms of air mass fraction and water temperature. Different water droplet size and thus injection quality, depending on the applied nozzle size, result in changing heat transfer between liquid and gas. At constant injected water volume flow, larger nozzle outlet diameter results in larger droplet size and thus decreasing heat exchange between water and air during the entire working cycle. Hereby at the expander's inlet, the mixture temperature after water injection corresponds to a thermal equilibrium between both fluids.
In Figure 3, indicator diagrams at male rotor circumferential speeds of 9.4 $m \cdot s^{-1}$ and 67.7 $m \cdot s^{-1}$ are presented for different injected water flow with respect to air mass fraction. Hereby, indicator diagrams at air mass fractions of

0.9 and 0.5 are compared with the dry-running operation. In terms of water injection, four significant mechanisms influence the screw expander operation and the pressure situation within the chamber during a working cycle. The first relevant effect on the expander's indicator diagram is the heat transfer from a liquid into an expanding gaseous phase. Due to its higher heat capacity, water increases the pressure level at a constant chamber volume by rising the chamber gas temperature. In Figure 3 considering the expanding chamber after passing over the inlet control edge, the effect of heat transfer can be observed in the indicator diagrams for both low and high male rotor circumferential speeds. Here, the higher the amount of injected water is, the higher the heat transfer and the pressure lift are.
The second significant effect of water injection on the time dependent chamber pressure results from blocking clearances within the screw expander. Theoretically, even low amounts of water partially block the clearances connecting two adjacent volumes in the expander, so they become "sealed" and the internal leakage declines. Hence, a pressure decrease can be expected after finishing the chamber filling, since the expanding chamber cannot be refilled by leakages from the following chamber at a higher pressure level. Nevertheless since the heat transfer effect seems to be more dominant with regard to pressure change, the chamber pressure in general increases for both male rotor circumferential speeds in Figure 3.

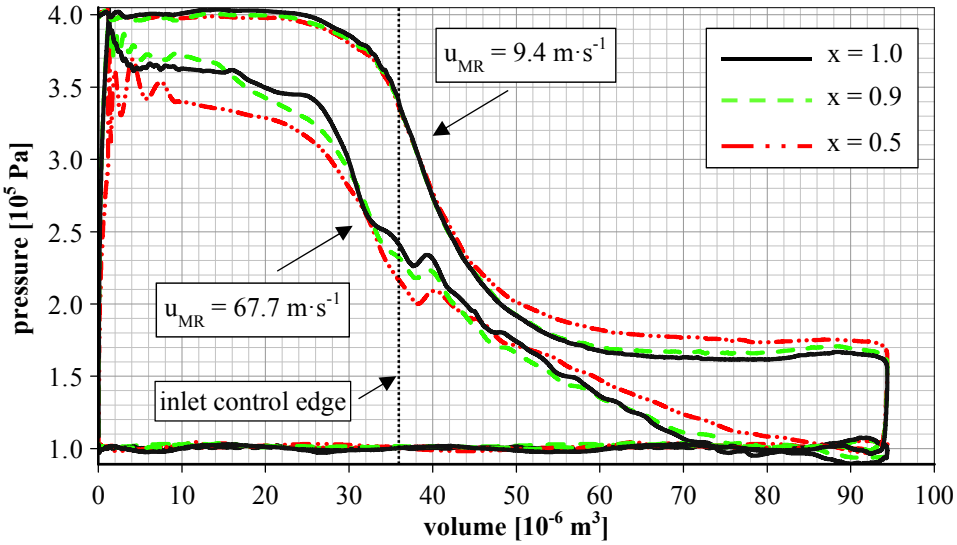

Figure 3: Indicator diagrams at male rotor circumferential speeds of 9.4 m·s^{-1} and 67.7 m·s^{-1}, different air mass fractions, inlet pressure of 4·10^5 Pa, air temperature of 90 °C, and water injection temperature of 60 °C

The third relevant influence mechanism is characterized by increasing inlet throttling at higher amounts of injected water due to declining speed of sound in terms of two-phase flow during the chamber filling. At higher male rotor circumferential speeds especially, reduced speed of sound results in a significant drop in pressure in the working chamber while it is connected to the inlet port.
The fourth important influence mechanism of water injection on the indicator diagrams results from hydraulic friction between water and the expander's rotors and casings due to the relatively high viscosity of the liquid compared to air. At this point primarily in the tight expander's clearances, dominant hydraulic frictional losses can be expected. Nevertheless, hydraulic friction losses cannot be directly evaluated by means of the indicator diagram at this point.
With respect to the pressure characteristic at a male rotor circumferential speed of 9.4 m·s^{-1}, the pressure drop during the chamber filling at increasing water flow results from a reduced speed of sound at the expander inlet. The adjacent pressure lift during the chamber expansion can be traced back to the increasing heat flow from the liquid into the air which dominates the clearance sealing effect. That means if heat exchange between both fluids can be neglected, the pressure level has, in general, to decrease due to reduced internal leakage.
Considering the indicator diagrams at a male rotor circumferential speed of 67.7 m·s^{-1}, a significant pressure drop over the inlet can be observed. Apart from particular inlet blocking by the liquid at the begin and end of chamber filling, a reduced speed of sound of the air-water mixture results in increasing inlet throttling. After the working chamber is disconnected from the inlet port, the chamber state mainly changes due to heat flow from water into air, lifting the chamber pressure level. Since the relevance of internal leakage is utterly low-dominant at high rotational

speeds, no significant pressure drop due to decreased internal leakage in this range can be expected. Due to heat input from the liquid into the air phase, no overexpansion can be observed at a male rotor circumferential speed of 67.7 $m \cdot s^{-1}$.

In Figure 3, a boundary effect of the time-dependent chamber pressure measurement is obvious at a male rotor circumferential speed of 67.7 $m \cdot s^{-1}$. Here at pressure metering position 1 up to a chamber volume of ca. $8 \cdot 10^{-6}$ m^3, acoustical Helmholtz resonances can be observed due to the sensor geometry as explained above.

The effect of water injection temperature is depicted in Figure 4. The indicator diagrams at both presented male rotor circumferential speeds are influenced by the liquid temperature. At low rotational speed which provides enough time to complete heat exchange between water and air and at which no significant hydraulic friction losses and inlet throttling can be expected, chamber pressure increases due to higher heat transfer from water into air at a constant chamber volume and increasing water temperature. Even if the time for heat flow and complete heat exchange at higher male rotor circumferential speed is not sufficient, higher chamber pressure can be observed at higher water injection temperatures. On the one hand, this can be traced back to declining inlet throttling due to the higher speed of sound at higher temperature levels. On the other hand, heat flow into air increases.

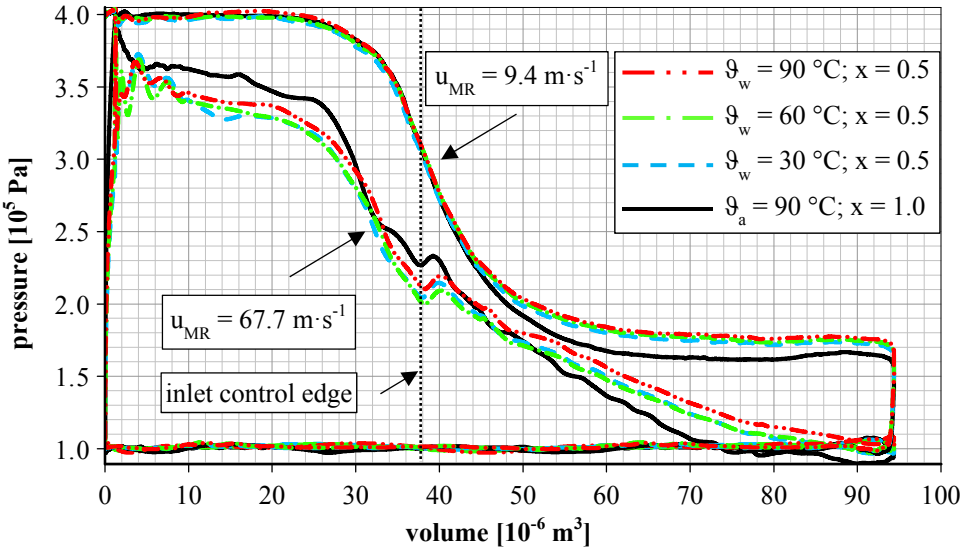

Figure 4: Indicator diagrams at male rotor circumferential speed of 9.4 $m \cdot s^{-1}$ and 67.7 $m \cdot s^{-1}$, inlet pressure of $4 \cdot 10^5$ Pa, air temperature of 90 °C, dry-running operation (x = 1), and different water injection temperatures at x = 0.5

5. CHARACTERISTIC DIAGRAMS

Characteristic diagrams of SE 51.2 are presented in Figure 5. Here, indicated power, solid and hydraulic friction losses, delivery rate, and mechanical efficiency as a function of male rotor circumferential speed at different air mass fractions and water temperatures are depicted.

With regard to indicated power determined from the indicator diagrams, a nearly linear increase in power up to a male rotor circumferential speed of 30 $m \cdot s^{-1}$ can be observed. Afterward, the power growth flattens out due to progressively increasing inlet throttling. Comparing different amounts of injected water, indicated power first slightly increases in relation to dry-running operation due to a chamber pressure rise resulting from heat input. However, at higher rotational speed and water flow, indicated power decreases since inlet throttling becomes more dominant. Here, an increasing inlet throttling in terms of reduced speed of sound seems to be the more dominant effect. With regard to decreasing water temperatures at an air mass fraction of 0.5, lower indicated power can be observed due to higher inlet throttling and lower heat input.

Friction losses represent the entire losses within the screw expander in terms of the relative movement of the screw expander's components. Here as expected, relatively low frictional losses occur at low rotational speeds independent of whether dry-running operation or water injection is considered and at which temperature water is injected. At increasing injected water flow and high expander's revolution speeds, hydraulic friction losses within the relatively tight clearances increase. In general, solid friction slightly increase at dry running (x = 1) and higher

rotational speeds. However, solid body friction between both rotors in the intermesh point seems to slightly decrease in the presence of a small amount of water (x = 0.9) presumably as a result of the more beneficial lubrication by water than dry air. With respect to water temperature, an increase in friction losses at lower water injection temperatures is obvious, which can be traced back to higher liquid's viscosity.
In terms of both dry-running operation and water injection, delivery rate decreases as a function of male rotor circumferential speed due to declining internal leakage and increasing inlet throttling. At the same time, an increase of water flow at low rotational speeds results in a significant drop of delivery rate according to more efficient clearance sealing. In contrast, increasing water flow at high rotational speeds reduces the delivery rate due to increasing inlet throttling. Considering water temperature, delivery rates do not change significantly (not presented here due to clarity reasons).

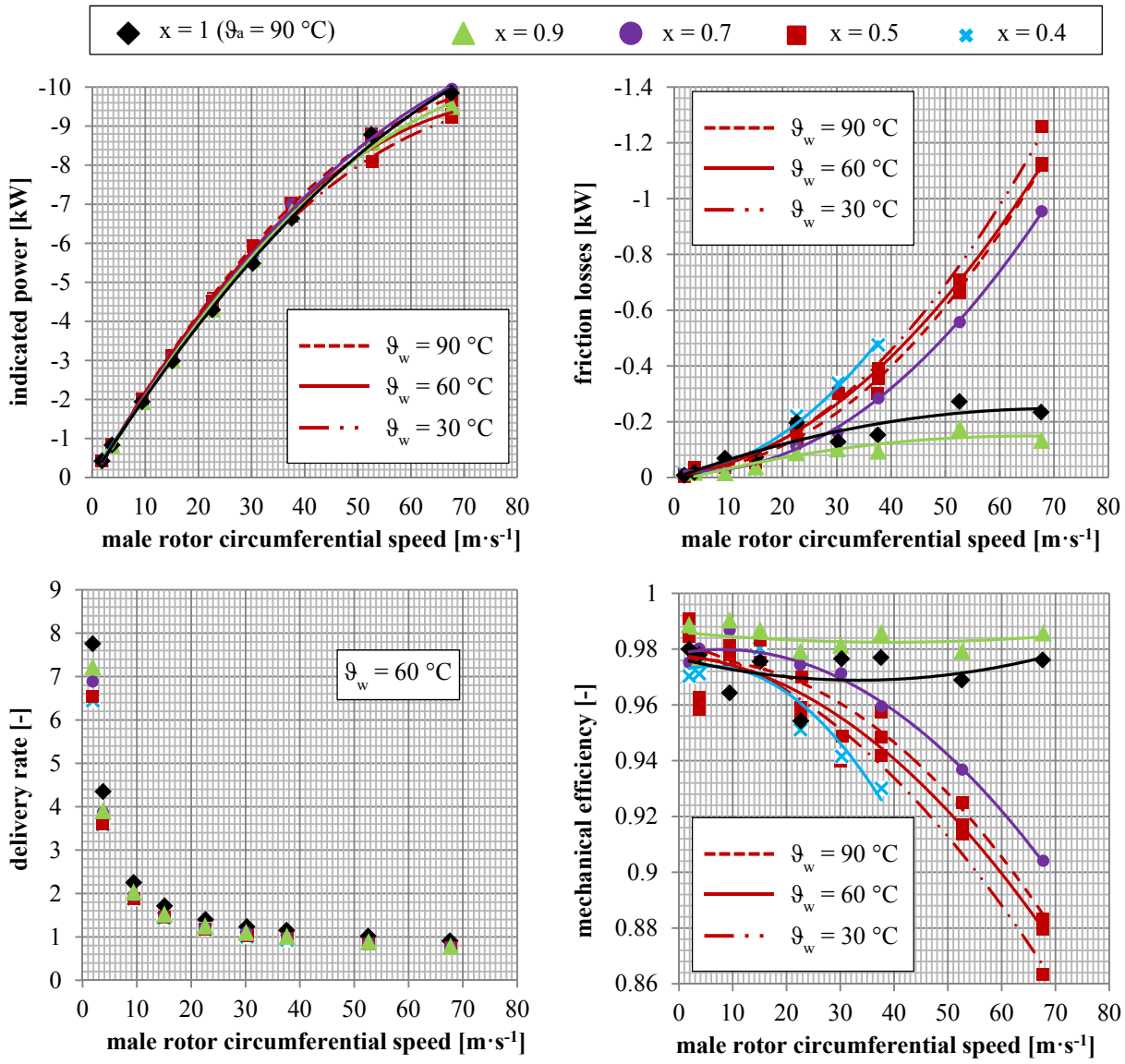

Figure 5: Indicated power, friction losses, delivery rate, and mechanical efficiency as a function of male rotor circumferential speed at different air mass fractions and water injection temperatures
(x = 0.5 at ϑ_w = 30 °C, ϑ_w = 60 °C, and ϑ_w = 90 °C; x = 0.9, x = 0.7, and x = 0.4 at ϑ_w = 60 °C)

Mechanical efficiency in Figure 5 represents the range of internal losses in the expander, including solid friction between both rotors, in the bearings and contact seals, as well as hydraulic losses due to water injection. With regard to a dry-running expander (x = 1), almost constant mechanical efficiency in the range between 0.97 and 0.99

can be observed. Here, no significant dependency on the rotational speed can be detected. Similar to the friction losses in Figure 5, mechanical efficiency first slightly increases at $x = 0.9$ and then systematically decreases, particularly at increasing air mass fraction and increasing rotational speeds. At higher water temperatures and a constant air mass fraction of $x = 0.5$, hydraulic friction declines and, thus, the mechanical efficiency increases moderately. Mechanical efficiency values deviating from the trend line with a second-degree polynomial used to approximate the progress of this characteristic number can be traced back to the mentioned issues evaluating the pressure measurement signals with respect to pressure distribution in the chamber during the chamber filling.
In summary, mechanical efficiency greater than 0.94 and relatively low mechanical losses even at very low air mass fraction and male rotor circumferential speeds up to 30 m/s are detected. In this characteristic operating range for liquid-injected screw expanders, satisfactory sealing of the clearances and heat input from the auxiliary fluid into the gaseous phase during expansion is available. At male rotor circumferential speeds greater than 30 $m \cdot s^{-1}$ hydraulic friction increases, so this range is not appropriate for wet-running expanders at high liquid flows.

5. CONCLUSION

This paper contains the results of an experimental investigation on indicator diagrams of a water injected twin-shaft screw-type expander SE 51.2. By means of the time-dependent chamber pressure distribution, relevant effects on the operational behavior of dry-running and liquid-injected screw expanders are presented.
Experimental investigations on water injected screw-type expanders by means of indicator diagrams show detailed information about the expander's operation with regard to the most relevant mechanisms resulting from water injection. The investigations provide a solid basis for validating and verifying models for hydraulic losses and heat transfer with respect to the operation of screw expanders. The aim of further investigations on liquid injected screw-type expanders is to provide an enhancement of the chamber model simulation tool KaSim developed at the Chair of Fluidics by Janicki (2007) with regard to adequate prediction of the aforementioned mechanisms.

REFERENCES

Cao, F., Gao, T., Li, S. Xing, Z., Shu, P. (2011). Experimental analysis of pressure distribution in a twin screw compressor for multiphase duties. *Experimental Thermal and Fluid Science, Volume 35, Issue 1, January 2011*, 219–225.

Gräßer, M. & Brümmer, A. (2014). An analytical model of the incompressible one-phase clearance flow in liquid injected screw expanders. VDI Bericht 2228, in *9th International Conference on Screw Machines 2014, Dortmund, Germany* (71–89).

Gräßer, M. & Brümmer, A. (2015). Influence of liquid in clearances on the operational behavior of twin screw expanders. In 9th *International Conference on Compressors and their Systems, IOP Conf. Series: Materials Science and Engineering 90 (2015)* 012060.

Janicki, M. (2007). *Modellierung und Simulation von Rotationsverdrängermaschinen*. Dissertation, TU Dortmund University, Germany.

Kliem, B. (2005). *Fundamentals of the Two-Phase Screw-Type Engine*. Dissertation, TU Dortmund University, Germany.

Kovacevic, A. & Rane, S. (2013). 3D CFD analysis of a twin screw expander. *8th International Conference on Compressors and their Systems, City University London.*

Nikolov, A. & Brümmer, A. (2014). Influence of water injection on the operating behaviour of screw machines. VDI Bericht 2228, in *9th International Conference on Screw Machines 2014, Dortmund, Germany* (43–60).

Ohman, H. & Lundqvist, P. (2015), Screw expanders in ORC applications, review and new perspective. In *3rd International Seminar on ORC Power Systems, Brussels, Belgium* (503–512).

Rinder, L., Kuchler, M., & Hackl, H. (2004), Water-Injection or Oil-Injection for Screw-Compressors in Comparison. *Schraubenmaschinen, Nr. 12 - 2004*, 65–74.

Rinder, L. & Moser, I. (1990). Untersuchung der Ölverteilung in den Arbeitsräumen naßlaufender Schraubenkompressoren. *VDI Berichte 859 - 1990*, 1–14.

Temming, J. (2007). *Stationärer und instationärer Betrieb eines unsynchronisierten Schraubenladers*. Dissertation TU Dortmund University, Germany.

Vasuthevan, H. & Brümmer A. (2016). Thermodynamic Modeling of Screw Expander in a Trilateral Flash Cycle. In *23rd International Compressor Engineering Conference at Purdue University*, number 1432.

Zellermann, R. (1996). *Optimierung von Schraubenmotoren mit Flüssigkeitseinspritzung.* Dissertation, TU Dortmund University, Germany.